2010, 12th International Conference on Optimization of Electrical and Electronic Equipment, OPTIM 2010

Multi–physical simulation of drive trains

Enno Lange, Michael van der Giet, Thomas Herold, and Kay Hameyer
Institute of Electrical Machines – RWTH Aachen University
Schinkelstrae 4, D-52056 Aachen, Germany
E–mail: Enno.Lange@IEM.RWTH-Aachen.de

Abstract—Converter fed and feedback controlled drive trains is today's standard configuration for highly dynamic drive applications. The design process for such drive trains must meet the target specifications as well as given constraints for the parasitic effects. Depending on the area of application, these parasitic effects require importance to be attached to e.g. sound radiation power, losses specific to the different components or the overall efficiency. Furthermore, understanding the inter-dependencies between converter, electric machine, gear and load is indispensable in the optimal design process.

I. Introduction

The first part of this paper gives an introduction to the simulation methods at hand and the different coupling schemes which are necessary to cope with the simulation of a complete drive train. Having a look at the electric machine supplied by the power electronic converter, it is obvious that the current wave form determines the working point of the machine, while the energy stored in the machine, thus the saturation, must be taken into account by the control of the converter. While this represents a physically strong coupled system, the numerical solution can be obtained in a weakly coupled manner.

The second part of the paper presents a complete simulation of a drive train beginning with the circuit simulation of the converter and its higher control coupled to the numerical field simulation of the machine and the behavior of the mechanical system. Herein, the applied field–circuit coupling and the system simulation is being presented in–depth. Additionally, the parasitic effects e.g. sound radiation of the electric machine and the overall efficiency of the drive train are derived. Finally, besides a summary, the simulations are to be compared with measurements.

TABLE I Physical quantities.

symbol	description
$\mathbf{I}$	vector of phase currents
$\mathbf{E}$	vector of electromotive forces
$\mathbf{L}^{\partial}$, $\mathbf{L}$	tangent and secant inductance matrix
P_l	unspecified losses due to parasitic effects
T	torque
n	rotational speed
F	local forces
σ	surface force density
u	local displacement in structure dynamics
v	surface velocity
p	sound pressure

The paper concludes with a discussion about the necessity of detailed system simulations.

II. Simulation Methods

Today's drive trains are assembled of

- the power electronic converter,
- the electric machine,
- the optional transmission gear and
- the load.

Several analytical and numerical tools for each of these components have been developed to support the design and optimization process. The overall optimization of the complete drive train may require to combine the specialized tools in order to reach the specified design goal, independently whether this is maximizing the efficiency or minimizing parasitic effects e.g. noise and vibration harshness or torque ripple.

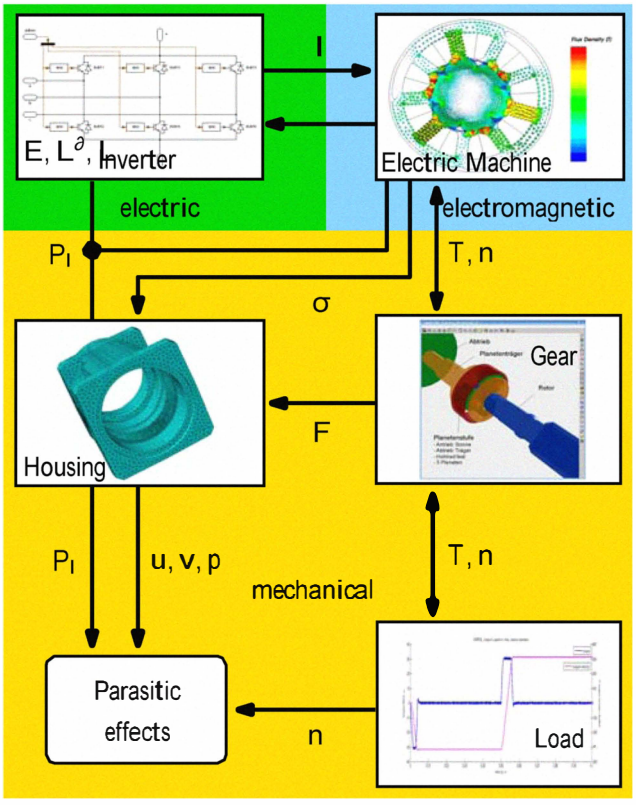

Fig. 1. Different coupled physical domains of the drive train: electric circuitry, electromagnetic field domain, mechanical domain.

TABLE II
OVERVIEW OF THE COMMON SIMULATION METHODS WITH RESPECT TO THE DIFFERENT COMPONENTS OF THE DRIVE TRAIN (THIS LIST IS NOT EX HAUSTIVE).

	drive train component	physical domain or property	simulation methods	Comment
1.	control strategy	control theory	ODE–solving environment	Commercial packages: Simulink, Portonus, Simplorer...
2.	electronic components of power converter	network theory, electric domain	– equivalent circuits (EC) – state space extraction – modified nodal analysis (MNA) – ...	Commercial packages: Plecs, Simplorer, Powersys, ... Open source: Qucs, SPICE, ... Ability for coupled simulation strongly depends on the package
3.	electric machine	slowly varying magnetic fields, electromagnetic domain	– magnetic equivalent circuit (MEC) – Boundary Element Method (BEM) – Finite Element Method (FEM) – ...	Commercial packages: Comsol, Flux, JMAG, Maxwell, Opera, ...
4.	transmission gear	gear design, mechanical domain	– Multi–Body systems – Finite Element Method – ...	Numerous commercial packages available

In a first step of system analysis, one needs to identify the physical quantities interconnecting the different components and their respective subdomains e.g. the housing of the machine or the gear/load. According to Fig. 1 the inverter is within the electric domain, the electric machine is within the electromagnetic domain and the housing, the gear transmission and the load can be assigned to the mechanical domain. The different domains interact by the physical quantities according to Table I. Note, for the sake of clarity Fig. 1 omits the control strategy.

In a following step, the model level of detail for each component must be chosen. This challenging part of the multi–physics simulation still requires a good knowledge of the complete system and the level of detail must be carefully chosen for each component in order to model all aspects and parasitic effects of interest. A brief overview of the simulation methods is given by Table II (with increasing level of detail of the simulation methods downwards). Here, the coupling of the different domains is implemented in a numerically weak basis as the physical coupling of the domains is weakly coupled as well allowing for different simulation methods and different time steps [1].

The following sections discuss the simulation methods necessary to perform a multi–physic simulation of the drive train according to Fig. 1 focusing on the electromagnetic domain with a lumped parameter extraction of the electric machine, the force calculation and the vibro–acoustic analysis of the housing within the mechanical domain.

A. Lumped parameter extraction of the electric machine

The simulation method of the electromagnetic domain is the Finite Element Method (FEM). Whenever the energy stored within the machine changes considerably, a new set of lumped parameters must be extracted from the FE model to account for this new state of operation of the machine [2]. Opposed to numerically strong coupled approaches of field–circuit coupled simulations [3]–[5], the weakly coupled approach allows for a co–simulation of different software packages. For the devices under study, a continuous evaluation of the energy flows of the electrical as well as the mechanical domain ensures a smooth extraction of the parameters, which is based on the balance of energy of the electrical machine, as presented in [6]. The machine is represented by a tangent induction matrix L^{∂}_{kj} of self and mutual inductances with dimension number of phases by number of phases and a vector of motion induced voltages E_k with dimension number of phases [7], [8]. The terminal voltage of phase k is given by the time derivative of the flux linkage ψ_k (with implicit summation over l):

$$\partial_t \psi_k = \partial_t \psi_{kl} + \partial_t \psi_f \tag{1}$$

Herein, $\psi_f = f(\alpha)$ is the remanence flux embraced by internal magnetomotive forces (mmf) being a function of the angular position of the rotor $\alpha = f(t)$, and $\psi_{kl} = f(\alpha, i_l)$ is the flux linkage in phase k depending on the current $i_l = f(t)$ carried by phase l and the rotor position α. Propagating the differential operator in (1), one yields:

$$\begin{aligned}
\partial_t \psi_k &= \partial_t (L_{kl} i_l) + \partial_t \psi_f \\
&= (\partial_t L_{kl})\, i_l + L_{kl}\, (\partial_t i_l) \\
&= (\partial_t i_l \partial_{i_l} L_{kl})\, i_l + \omega\, (\partial_\alpha L_{kl})\, i_l + L_{kl}\, (\partial_t i_l) + \partial_t \psi_f \\
&= \partial_t i_l\, ((\partial_{i_l} L_{kl}) i_l + L_{kl}) + \omega (\partial_\alpha L_{kl}) i_l + \omega \partial_\alpha \psi_f \\
&= (\partial_t i_l)\, L^{\partial}_{kl} + \omega \partial_\alpha \psi_k .
\end{aligned} \tag{2}$$

The first term of the terminal voltage (2) expresses the induced voltage by the flux linkage described by the tangent inductance matrix L^{∂}_{kl} and the second term the motion induced voltage being proportional to the angular velocity ω respectively. This approach has been investigated and a verification benchmark has been designed and evaluated in [9]. The extraction of these lumped parameters from the set of FE equations is explained in the following section.

1) Extraction of the tangent inductance matrix : Let

with the right hand–side (implicit summation over l)

$$b_i = \int_\Omega \mathbf{j}\cdot\alpha_i = i_l \int_\Omega w_l\cdot\alpha_i := i_l W_{il}, \qquad (4)$$

be the nonlinear FE equations describing the machine with internal magnetomotive forces (i.e. permanent magnets) and stator currents. Herein, $\mathbf{j}$ is the current density and α_i are the shape functions of the Galerkin scheme. The magnetic vector potential is given by a and $\mathbf{M}$ is the non–linear system matrix arising from the Galerkin scheme. In 2D, the current shape functions become $w_k = \frac{w_l}{A_l} e_z$ with w_l being the turns of phase l and A_l the corresponding turn area. In 3D, the current shape functions are following the threads of the coil winding. According to (4), W_{il} is defined as the current shape vector.

Now, let i_j^* be the currents at time t, and $b_i^* = i_j^* W_{il}$ the corresponding right–hand sides. Solving (3) with $b_i \equiv b_i^*$ and i_j and a first order a fixed rotor angular position $\delta\alpha = 0$ gives a linearization around this particular solution writes

$$J_{ij}(a_j^*)\,\delta a_j = b^*_i - b_i(a_j^*),$$

with the Jacobian matrix $J_{ij} \equiv \partial_{a_j} M_{in}(a_j)^* a_n$.* Since $(a^*)_j = b_i^*$, one has

$$J_{ij}(a_i^*)\;\delta a_i|_{\delta\alpha=0} = \delta b_i. \qquad (6)$$

One can now repeatedly solve (6) with the right–hand sides $\delta b_i = \delta i_l W_{il}$ obtained by perturbation of one after the other m phase currents i_l and obtain m solution vectors for $\delta a_j|_{\delta\alpha=0}$. Since (6) is linear, the magnitude of the perturbations δi_l is arbitrary. In this way, one can define by inspection the tangent inductance matrix L^∂_{kl} of the electrical machine seen from terminals as

$$= W_{kj} J_{ji}^{-1}(a_j^*) W_{il}\;\delta i_l, \equiv L^\partial_{kl}\;\delta i_l, \qquad (7)$$

with

$$L^\partial_{kl} = W_{kj} J_{ji}^{-1}(a_i^*) W_{il}. \qquad (8)$$

2) Extraction of the motion induced voltage: One can now complement (2) to account for the electromotive force (emf):

$$\partial_t \psi_k = L^\partial_{kl}\partial_t i_l + \omega E_k \qquad (9)$$

with $E_k \equiv \partial_\alpha \psi_k$. The direct computation of the α derivative requires to slightly shift the rotor, re–mesh, solve the FE problem, evaluate new fluxes and calculate a finite difference. In order to avoid this tedious process, one can again call on the energy principles. One has

$$E_k = \partial_\alpha \psi_k = \partial_\alpha \partial_{i_k} \Psi_M = \partial_{i_k}\partial_\alpha \Psi_M = \partial_{i_k} T \qquad (10)$$

where T is the torque and Ψ_M is the magnetic energy of the system. During the identification process described by (7), it is thus easy to calculate additionally the torque corresponding to the perturbated solutions $\delta a_j|_{\delta\alpha=0}$, and to evaluate the motion induced voltage E_k of each phase k as the variation of torque with the perturbation of the corresponding phase current i_k.

Beware however that, as the torque is a nonlinear function of the fields, the perturbations need in this case to be small. Because of the linearity of (6), one may scale the perturbation currents in (10) which yields:

$$E_k = \frac{T(a_i^*) - T(a_j^* + \lambda\delta a_j|_{\delta\alpha=0})}{\lambda\delta i_k} \text{ with } \lambda = \kappa\frac{\|a_i^*\|_2}{\|\delta a_j\|_2}. \qquad (11)$$

Herein, the scale factor is chosen between $0.01 \le \kappa \le 0.05$.

B. Force calculation

With the field distribution obtained form the field–circuit coupled simulation, the next step is to determine the electromagnetic force excitations.

Magnetic forces acting on a given medium are the divergence of the electromechanical tensor of that medium. Each medium has its own electromechanical tensor, and that of empty space, or air, is the well known Maxwell stress tensor [10]. In consequence, magnetic forces come under volume– and surface–density form. In saturable non–conducting materials, the volume density is basically related with the gradient of the magnetic reluctivity, and it is usually negligible with respect to the surface–force density $\Delta\sigma$. The latter, located at material discontinuities (e.g. on the stator surface in the air gap), is the divergence in the sense of distribution of the electromechanical tensor. It can be shown [11] that it has a normal component only, whose amplitude is

$$\Delta\sigma_n = [b_n(h_{1n} - h_{2n}) - (w_1^0 - w_2^0)], \qquad (12)$$

where b_n is the normal component of the magnetic flux density b at the interface between the stator and the air gap. h_{1n} and h_{2n} are the normal components of the magnetic field strength h in the air and in the stator iron, respectively. The magnetic co–energy density w^0 is related to the magnetic energy density w by

$$w^0 = h(b)\cdot b - w(b) = h(b)\cdot b - \int_0^{|b|} |h(x)|dx. \qquad (13)$$

Due to the constant magnetic permeability of air, w_1^0 is

$$w_1^0 = h\cdot b - \frac{1}{2}h\cdot b = \frac{|b|^2}{2\mu_0}, \qquad (14)$$

where μ_0 denotes the magnetic permeability of vacuum. As the magnetic steel sheets have a nonlinear magnetic characteristic, the magnetic force density is calculated by integrating the magnetic co–energy density w_2^0 in (12) along the magnetic flux density.

If the permeability of the iron can be considered to be constant, (12) can be simplified to

$$\Delta\sigma_n = \frac{1}{2}[b_n(h_{1n} - h_{2n}) - h_t(b_{1t} - b_{2t})]. \qquad (15)$$

C. Vibro–acoustic analysis

1) Structure dynamics : The deformation–solver formulation is constructed using Hamilton's principle. After discretizing, the general vibration equation in frequency domain is obtained

$$(\mathbf{K} + \mathbf{j}\omega\mathbf{C} - \omega^2\mathbf{M}) \cdot \underline{\mathbf{d}}(\omega) = \underline{\mathbf{f}}(\omega), \qquad (16)$$

where $\mathbf{K}$, $\mathbf{C}$ and $\mathbf{M}$ are the global stiffness and damping and mass matrix, respectively. The imaginary number is denoted by $\mathbf{j}$ and ω describes the angular frequency of the problem. $\underline{\mathbf{d}}(\omega)$ is the vector of the complex nodal deformation, and $\mathbf{f}(\omega)$ is the complex excitation force vector. As electrical machines typically can be considered low damped systems [12], the term $\mathbf{j}\omega\mathbf{C}$ is typically disregarded, as it is done in this work.

The complex surface–force density $\Delta\underline{\sigma}_n(\omega)$ is transformed from the electromagnetic simulation to a nodal force $\underline{\mathbf{f}}_k(\omega)$ on the mechanical model for each frequency to be analyzed. The force at node k is given by

$$\underline{\mathbf{f}}_k(\omega) = \sum_{j=1}^{n_e} \Delta\underline{\sigma}_{nj}(\omega) \int_{\Omega_m} \rho_j N_k e_n \, d\Omega_m, \qquad (17)$$

where n_e is the number of elements of the electromagnetic mesh, $\Delta\underline{\sigma}_j(\omega)$ is the surface–force density on the j–th element, e_n is the unit-normal vector, Ω_m is the mechanical domain, ρ_j and N_k are the element and nodal shape functions, respectively [13].

Then, the structure–dynamical simulation is performed. This can be done either by solving (16) directly for each individual frequency separately, or by performing a modal analysis and the corresponding [14], i.e. finding the eigenvalues ω_i^2 eigenvectors Φ_i in mass normalized form of the eigenproblem

$$\mathbf{K}\mathbf{d}(\omega) = \omega^2\mathbf{M}\mathbf{d}(\omega), \qquad (18)$$

together with a subsequent modal superposition

$$\underline{\mathbf{d}}(\omega) = \sum_{i=1}^{N} \frac{\underline{\Phi}_i \underline{\mathbf{f}}(\omega)^T \Phi_i}{\omega_i^2 - \omega^2}, \qquad (19)$$

where N is the number of eigenvalues. The latter approach is used in this work.

2) Acoustic radiation : For the acoustic simulation, the mechanical deformation of the electric machine is converted to the velocity ($\underline{\mathbf{v}} = \mathbf{j}\omega\underline{\mathbf{d}}$). In principle, the calculation of acoustic fields is possible with the FEM. However, for calculation of air–borne noise this method is unfavorable, since the entire calculation area has to be discretized. An alternative is offered by the boundary element method (BEM). Here, only the surface of the housing of the electric machine is discretized. The basic principle of the BEM is the solution of the Helmholtz differential equation

$$\Delta\underline{\mathbf{p}} + k^2\underline{\mathbf{p}} = 0, \qquad (20)$$

with the complex sound pressure p and the wave number $k = \omega/c$ [15]. Here, c is the sound velocity of air. After further calculation the following system results

$$\underline{\mathbf{H}} \cdot \underline{\mathbf{p}} = \underline{\mathbf{G}} \cdot \underline{\mathbf{v}}. \qquad (21)$$

$\underline{\mathbf{H}}$ and $\underline{\mathbf{G}}$ are system matrices and the complex velocity vector $\underline{\mathbf{v}}$ serves as the excitation value to the problem. A numerical solution of (21) results in the sound–pressure vector $\underline{\mathbf{p}}$. For the use of this method an acoustic model of the radiating surface is needed. To decrease the numerical effort, the internal surface of the housing of the electric machine is not included in the model. Therefore, the acoustic model consists of the simplified outer surface of the machine's housing without holes. The mechanical velocity of the housing is transferred to this acoustic mesh [16].

Since the BEM is applied, sound–pressure and sound–particle velocity are evaluated on predetermined points or surfaces. As integral quantities the acoustic power and the sound intensity of the machine are calculated. The results are available at discrete frequencies.

III. Drive train simulations

During many research projects and in cooperation with different companies the simulation methods presented in the previous chapter have been applied and models with different levels of detail have proven their feasibility. Within this chapter, selected multi–physics discipline applications of technical and physical importance are presented and their features are pointed out.

A. Automotive claw pole alternator

Due to its irreducible 3D flux path structure and the connected bridge rectifier, the claw pole generator is a challenging field–circuit coupled system [17]. It can be solved either by permeance models, state space models or the numerically weak or strong coupled method. Here, the numerically weakly coupled approach is chosen and a temporary lumped parameter representation of the alternator, seen from stator terminals, is extracted from the Jacobian matrix of the linearized FE model. This lumped parameter representation of the machine is then incorporated into a circuit simulator based on the Modified Nodal Analysis (MNA) [18].

1) Transient coupling scheme: The numerically independent solution process of the circuit and the field problem requires a time stepping scheme synchronizing the MNA

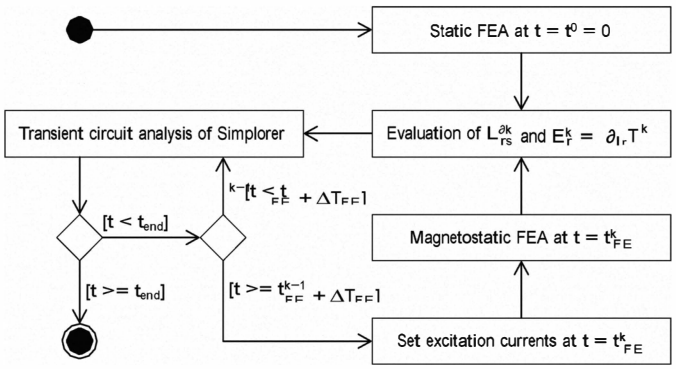

Fig. 3. Flowchart of the transient coupled simulation with static time stepping.

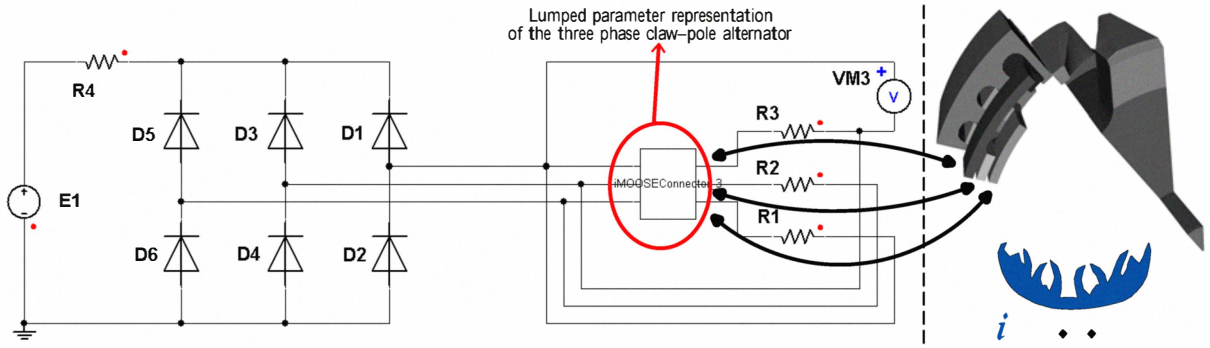

Fig. 2. Application of the proposed coupling: three phase claw–pole alternator connected to a rectifier working on a constant voltage source.

and the FE analysis (FEA). A basic scheme is presented in Fig. 3. Herein, the time step ΔT_{FE} of the FE–system is constant. By starting the simulation, the initial values of the tangent inductance matrix $L^{\partial 0}_{rs}$ and the induced voltages E^0_r are calculated by a magneto–static FEA for each phase r and incorporated into the equation system of the circuit simulator. If the circuit simulator reaches $t >= t^{k-1}_{FE} + \Delta T_{FE}$, a new set of phase currents is imposed, the time step of the circuit simulator can be adapted according to the topological changes in the external circuit caused by e.g. switching power electronic components.

2) Realization of coupling: Any circuit simulator in combination with a magnetostatic FE–solver can be used provided both packages have proper interface capabilities. In this work, the circuit simulator Simplorer [19] and the IEM in–house FE software package iMOOSE [www.iem.rwth-aachen.de] have been used. Simplorer provides a C–Interface giving access to different stages of the time stepping scheme. Since iMOOSE is written in C++, the package is flexible and can be linked to any given library.

For the field and circuit simulations running on different operating systems, and in order to avoid tedious and error–prone data exchange via files, a network based data exchange has been implemented. To reduce the implementation effort to a minimum, while preserving maximum flexibility, the communication is based on the free implementation omniORB [20] of the CORBA[1] standard. The CORBA standard defines a platform independent interface definition language, by which remote procedure calls are being made transparent to the program designer. Thereby, the program designer need not to worry about the implementation of the complete network stack.

The basic implementation is outlined in Fig. 4. Simplorer is extended by a user library which incorporates the extracted lumped parameters L^{∂}_{rs} and E_r from iMOOSE into the equation system of Simplorer. In turn, the actual phase currents I_r are submitted to iMOOSE along with a set of control parameters. All communication is done via the standard network.

3) Simulation of the claw pole alternator: The proposed coupling approach is applied to a three phase claw–pole alternator which is connected via a B6–bridge D1–D6 to the constant voltage source E1 representing the battery in series with the resistance R4, Fig. 2. The alternator's winding resistances are labeled R1 to R3. The excitation current is assumed to be constant in this simulation, and is modeled as internal magnetomotive force.

The emf of the claw pole alternator is calculated both by finite differences a) and by the energy approach b) (Sec. II-A2) and included within rectifier topology given by Fig. 2. The simulated and measured output currents are shown in Fig. 5. While implementation a) performs well at low rotation speeds, the simulated current for the highest speed clearly exceeds the measurements. Implementation b) appears to have a small offset compared to the measurement.

Due to its fragile nature, implementation a) is unfavorable because the calculated induced voltage is very sensible to the chosen shift of the rotor. The offset of the implementation b) might stem from the calculation of the torque by the Maxwell stress tensor. A verification and comparison with different approaches of the calculation of the torque will provide useful additional information. All simulations deliver an output current higher than the measured one.

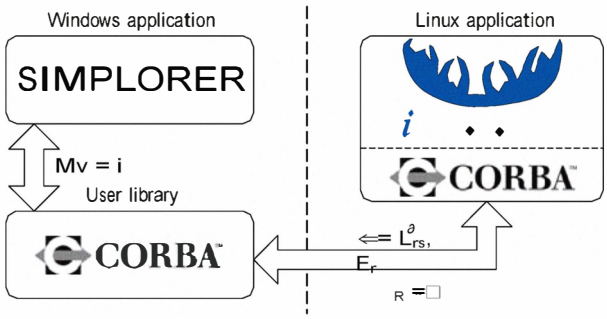

Fig. 4. Simulation infrastructure communicating via the CORBA standard.

[1]CORBA R is a registered trademark and the CORBA Logo™ is a trademark of the Object Management Group, Inc.

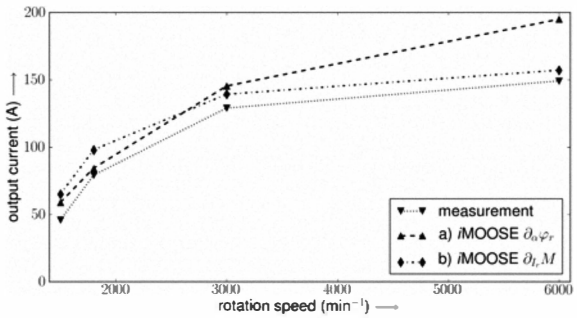

Fig. 5. Comparison of the mean output currents of the claw–pole alternator.

4) Discussion: The numerically weak coupling as presented in section II-A is applicable to simulate complex three dimensional field–circuit problems such as the claw–pole alternator. Two approaches to calculate the motion induced voltages are implemented. Besides the good accordance between simulated and measured currents, the energy based approach is numerically stable. Though the calculation of the torque is crucial for this approach, it appears to be more reliable than the calculation of the emf by finite differences. The communication between Simplorer and iMOOSE via network avoids error prone file locking mechanisms necessary for synchronizing the solution process and additionally bridges the different operating systems. Furthermore, the weak coupling reduces the computation time when compared to numerically strong coupled approaches providing good results. During a standard simulation cycle the circuit simulator performs 10 times more transient steps before a new FE extraction is calculated. Thus, when compared to numerically strong coupled approaches a significant saving of time is achieved.

B. Acoustic performance of a switched reluctance drive (SRM)

While the previous application of the claw pole alternator did not include any control loop, the following example of the switched reluctance machine (Fig. 6) requires a closed loop control and is combined with a multi–physics simulation of the acoustic radiation of the machine. The rotor of the SRM has an asymmetric pole geometry to improve start–up torque. The pole shape has been optimized subject to low torque ripple in a previous study [21]. The analysis focuses on the impact of the optimization on the overall acoustic behavior due to the rotor shape optimization. The field–circuit coupling is based the temporary lumped parameter model of the magnetic part incorporated into the circuit simulator Simplorer (s. section II-A). The harmonic force excitation is calculated by means of Maxwell's stress tensor computation (section II-B) and transformed to the mechanical mesh by mapping techniques. The structure dynamic problem is solved in the frequency domain using Finite Element modal analysis and super–position. The radiation characteristic is obtained from boundary element acoustic simulation (section II-C).

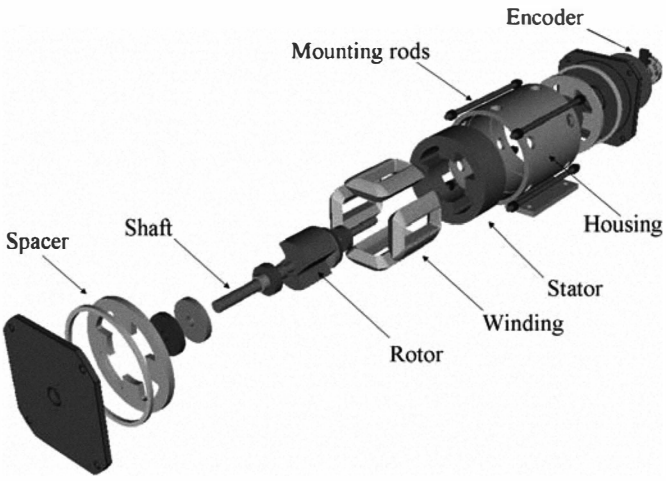

Fig. 6. Mechanical model of the SRM.

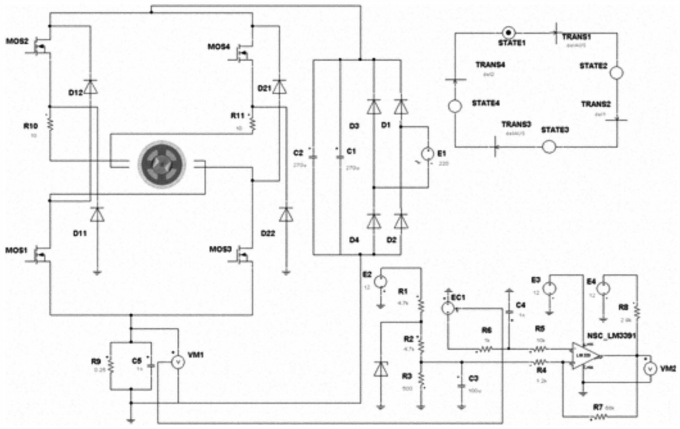

Fig. 7. Circuit model of the SRM with power electric circuit.

1) Circuit simulator: For the device under study, this is realized by an analog regulation loop in practice. Thus, the complete circuitry including the control as well as the hysteresis control is modeled within the used circuit simulator Simplorer [19]. The hysteresis control is implemented by means of Simplorer featured state machines (see upper right of Fig. 7).

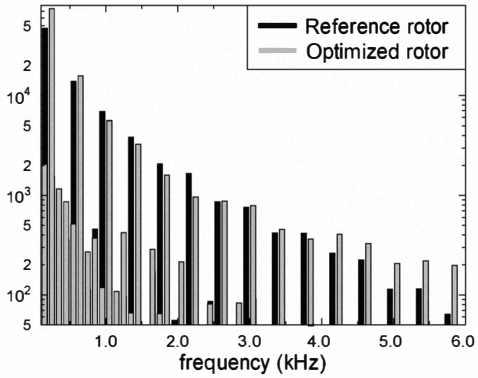

Fig. 8. Simulated force density with mode r = 2 of the SRM.

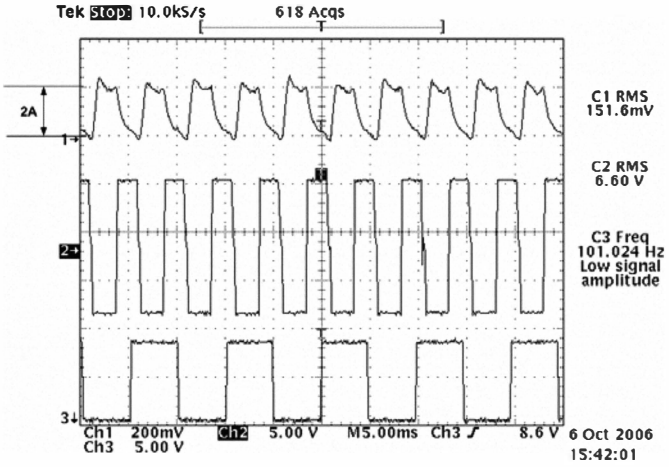

Fig. 9. Measured currents of the SRM.

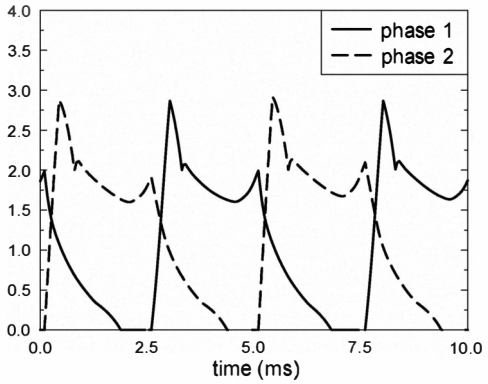

Fig. 10. Simulated currents of the SRM.

The currents of the optimized rotor shape form are simulated by the field circuit–coupled model and compared with measurements. A sufficient agreement between simulated and measured currents can be noted.

2) Acoustic simulation: Since the force excitation, driven by the current, has a rectangular waveform, the higher harmonics are decaying with the frequency. For example, the spectrum of the circumferential mode $r = 2$ is shown in Fig. 8. It can be seen, that in the frequency range up to 4 kHz, the optimized rotor shows better or approx. equal performance in terms of force excitation. However, in the range between 4 kHz and 6 kHz the force excitation of the optimized rotor is higher. Because no clear statement about the influence of the rotor geometry on the acoustic behavior can be made from force excitation alone, a numerical modal analysis is performed, and the eigenvalues within the frequency range of interest are being identified.

Because the radiation characteristic mostly differs in magnitude rather than in shape for the reference and the optimized rotor, the total acoustic power level is calculated to directly compare both designs. Since the reference rotor gives 46.7 dB and the optimized rotor 47.4 dB, it can be concluded that in overall both designs have comparable acoustic behavior.

TABLE III
COMPARISON OF SRM WITH REFERENCE AND OPTIMIZED ROTOR.

Value	Reference rotor	Optimized Rotor
Max. phase current (A)	2.85	2.87
Mean phase current (A)	1.31	1.14
Max. torque (Nm)	0.823	0.385
Mean torque (Nm)	0.284	0.267
Torque ripple (Nm)	0.788	0.303
Total sound power level (dB)	46.7	47.4

3) Discussion: As this study is comparing a rotor type that has been optimized for torque ripple with its reference counter–part, a final comparison is given in Table III. It clearly highlights that the optimization is effective, since the side effects, such as decrease of mean torque and increase of total acoustic power are acceptable.

C. Simulation of PMSM servo drive

Creating the simulation environment of a PMSM requires the different components to be modeled in their respective simulation domains. In case of the examined servo drive these components are the machine, the control, and the power electronic converter. The control is represented by an analytical simulation (AS) within the graphical simulation environment Simulink™ [22] solving ordinary differential equations (ODE). The inverter is modeled in the circuit simulation (CS) tool Plecs™while the numerical field computation is performed by the IEM FE–software package iMOOSE. The fundamental platform for the overall simulation is based on Simulink as well. Fig. 11 shows an overview of the entire simulation environment. While the electrical and mechanical equations and the control are embedded in the analytical solver platform Simulink the circuit simulation and the FEA are additionally attached. These parts, i.e. the CS, the FEA, the electrical and mechanical equations together, and the trigger control, represent the field–circuit (FC) coupling (dashed box). In the following a view aspects are enlarged and the parameter and signal exchange is explained.

1) Trigger control: The trigger control is an important aspect of the field–circuit coupled simulation. Here, the time step of the FEA is determined. The implemented FC is based on the weak coupling implying different step sizes for the circuit simulations and the FEA. This may save a lot

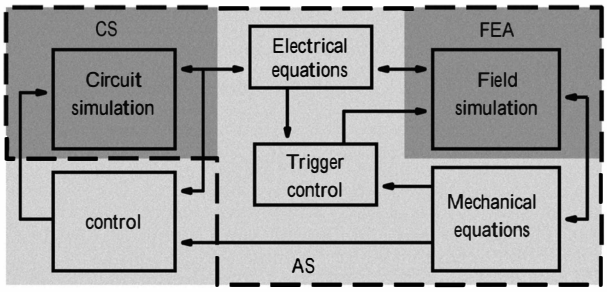

Fig. 11. Field circuit coupling scheme including control strategy of the PMSM.

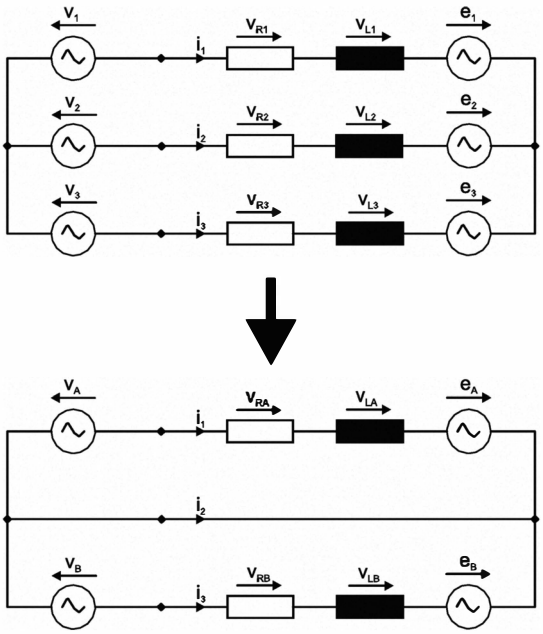

Fig. 12. Reduction of circuit elements of the PMSM circuitry.

of computational effort since the time constant of the field domain τ_{FE} usually exceeds the time constant of the circuit domain τ_{AS} by orders of magnitude and thus the relation of the time step is $\Delta T_{FE} >> \Delta T_{AS}$. A reasonable accounting for this relation is to adapt the time step. This can be done by energy considerations. Whenever the energy in the system is changing by a certain amount the trigger control gives the signal for extracting a new set of lumped parameters from the FEA. The energy in the system is divided up in four parts:

- The total electrical energy supplied through the terminals.
- The energy of the ohmic losses in the windings.
- The magnetic energy stored in the field.
- The mechanical energy driven by the shaft.

Whenever the total energy changes by a given threshold, a new set of lumped parameters is being extracted and supplied within the calculation of the electrical equations. To ensure that position dependent influences are not neglected while the total change of the energy remains below the threshold, an additional trigger condition for the position is accounting for the motion of the rotor.

2) Electrical equations: Since the circuit simulator Plecs is based on a piece–wise linear state–space approach, the circuit equations are represented by a set of time–invariant equations [23]. For the given three phase system of the PMSM according to Fig. 12, the lumped parameter inductance matrix extracted from the FEA is represented by controlled current sources leading to over–determined equation system within Plecs. To surmount this over–determination one may reduce the equivalent circuit elements as shown in Fig. 12. This reduction takes place within the AS domain of the field circuit coupling and the calculated currents are transferred to the CS domain via signal controlled current sources (see Fig. 11).

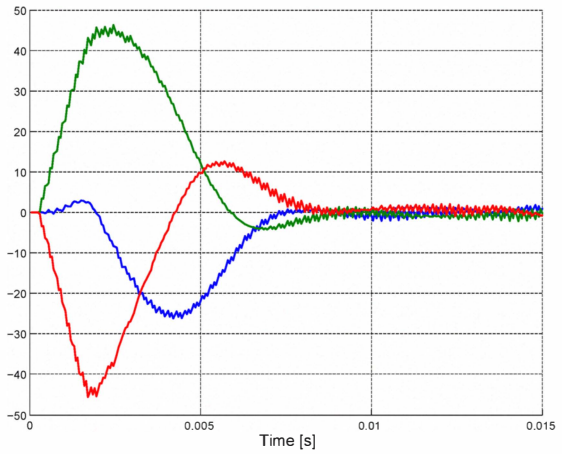

Fig. 13. Simulated stator currents of the PMSM during start up.

3) Simulation and Measurements: In order to make the simulated and measured time values comparable, the control of the power electronics of the inverter is running on the rapid prototyping system dSPACE [24] using the Simulink environment. The FC is replaced by the I/Os of the dSPACE board building a software–in–the–loop platform. The current waveforms of start up of the PMSM under no–load condition are simulated (Fig. 13) and compared to the measured current waveforms of the test bench running exactly the same control strategy as of the simulation (Fig. 14).

4) Discussion: Although the basic shapes of the plots are quite similar there are however notable deviations. At first the maximum currents have a difference of approx. 20%. Moreover, the PWM influence on the simulated currents is more distinctive, whereas the measurements seems to have a low–pass characteristic. Further investigations regarding the circuit modeling are supposed to explain this behavior, since the driver circuitry of the IGBT is neglected and the IGBT themselves are supposed to be ideal switches.

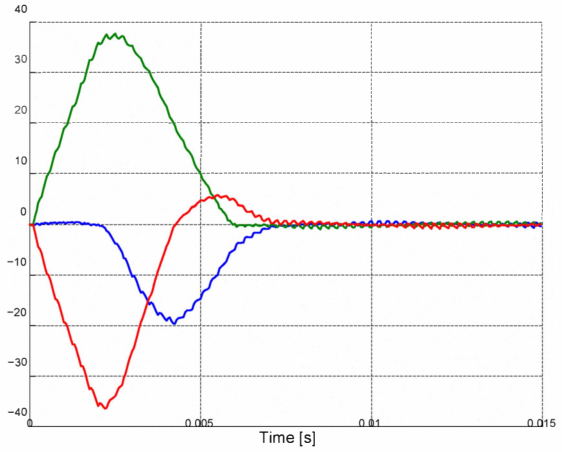

Fig. 14. Measured stator currents of the PMSM during start up.

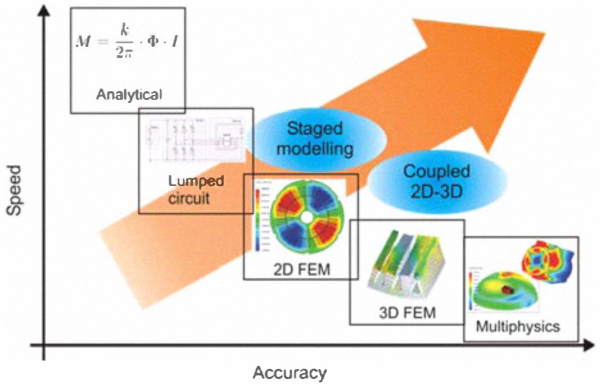

Fig. 15. Speed vs. accuracy: From analytical to multiphysics.

IV. Conclusions

The multi–physical simulation of drive trains is an important aspect and a discipline with a valuable contribution in the optimization process. This paper is focused on the coupling of the electric and electromagnetic domain including the power electronic converter and the electric machine with its controls. The lumped parameter extraction of the electric machine is explained as well as the vibro–acoustic simulation tool chain. Furthermore, three different application examples are given.

The claw pole alternator is simulated in combination with its bridge rectifier to calculate the output current. The numerical weakly coupled simulation allows for a great saving of computation time.

The second application of an SRM compares the acoustic performance of a previously optimized rotor with its original design and is modeled by a field–circuit coupled simulation followed by a structure–dynamic FEM simulation and a BEM simulation to obtain the sound pressure and the particle velocity.

A PMSM servo drive as the third application combines the field–circuit coupled simulation with the optimal design of the control strategy which is being transferred by a prototyping platform to a software–in–the–loop system.

Though the presented multi–physics simulation have proven its value throughout the optimization with respect to the design goals, one needs to keep in mind the ratio of simulation speed and accuracy as shown in Fig 15. Also, with the increasing level of detail the required knowledge to accurately build the models within their physical domains is increasing as well. Thus, for a successful multi–physics simulation of a drive train a good knowledge of the simulation tools at hand for each physical domain is almost indispensable, usually being distributed amongst different persons of a research or development team.

References

[1] K. Hameyer and R. Belmans, Numerical Modelling and Design of Electrical Machines and Devices, ser. Advances in Electrical and Electronic Engineering. WIT Press, Southampton, 1999.

[2] E. Lange, F. Henrotte, and K. Hameyer, "A circuit coupling method based on a temporary linearization of the energy balance of the finite element model," Magnetics, IEEE Transactions on, vol. 44, no. 6, pp. 838–841, June 2008.

[3] T. Dreher, R. Perrin-Bit, G. Meunier, and J. Coulomb, "A three dimensional finite element modelling of rotating machines involving movement and external circuit," Magnetics, IEEE Transactions on, vol. 32, no. 3, pp. 1070–1073, May 1996.

[4] P. Leonard, H. Lai, and R. Hill-Cottinhgam, "Treatment of symmetry in three dimensional finite element models of machines coupled to external circuits," Energy conversion, ieee transactions on, vol. 14, no. 4, pp. 1276–1281, Dec 1999.

[5] A. Canova, M. Ottella, and D. Rodger, "A coupled field-circuit approach to 3d fem analysis of electromechanical devices," Electrical Machines and Drives, 1999. Ninth International Conference on (Conf. Publ. No. 468), pp. 71–75, 1999.

[6] F. Henrotte and K. Hameyer, "The structure of electromagnetic energy flows in continuous media," Magnetics, IEEE Transactions on, vol. 42, no. 4, pp. 903–906, April 2006.

[7] N. Demerdash and T. Nehl, "Electric machinery parameters and torques by current and energy perturbations from field computations. i. theory and formulation," Energy conversion, ieee transactions on, vol. 14, no. 4, pp. 1507–1513, Dec 1999.

[8] E. Lange, F. Henrotte, and K. Hameyer, "An efficient field-circuit coupling based on a temporary linearization of fe electrical machine models," Magnetics, IEEE Transactions on, vol. 45, no. 3, pp. 1258 –1261, march 2009.

[9] M. van der Giet, E. Lange, and K. Hameyer, "TESTCASE: a benchmark problem for coupled field-circuit simulations," COMPEL: The International Journal for Computation and Mathematics in Electrical and Electronic Engineering, vol. 28, no. 3, pp. 668–681, 2009.

[10] F. Henrotte and K. Hameyer, "A theory for electromagnetic force formulas in continuous media," Magnetics, IEEE Transactions on, vol. 43, no. 4, pp. 1445–1448, April 2007.

[11] J. Melcher, Continuum Electromechanics. MIT Press Cambridge Massachusetts, 1981.

[12] J. Yang, S, Low-noise electrical motors, J. Yang, S, Ed. Clarendon Press Oxford, 1981.

[13] O. Zienkiewicz and R. Taylor, The Finite Element Method, 4th ed. McGraw-Hill Book Company, London, 1991, vol. 2 - Solid and Fluid Mechanics Dynamics and Non-linearity.

[14] S. Long, Z. Zhu, and D. Howe, "Vibration behaviour of stators of switched reluctance motors," Electric Power Applications, IEE Proceedings -, vol. 148, no. 3, pp. 257–264, May 2001.

[15] R. D. Ciskowski and C. A. Brebbia, Boundary element methods in acoustics. Elsevier, 1991.

[16] M. Furlan, A. Cernigoj, and M. Boltezar, "A coupled electromagnetic-mechanical-acoustic model of a dc electric motor," COMPEL: The International Journal for Computation and Mathematics in Electrical and Electronic Engineering, vol. 22, no. 4, pp. 1155–1165, 2003.

[17] E. Lange, M. van der Giet, F. Henrotte, and K. Hameyer, "Circuit coupled simulation of a claw-pole alternator by a temporary linearization of the 3d-fe model," in Electrical Machines, 2008. ICEM 2008. 18th International Conference on, sept. 2008, pp. 1 –6.

[18] C. W. Ho, A. E. Ruehli, and P. A. Brennan, "The modified nodal approach to Network Analysis," IEEE Transactions on Circuits and Systems, vol. 22, no. 6, pp. 504–509, June 1975.

[19] ANSYS Inc., "Simplorer: System simulation software for multi-domain design," http://www.ansoft.com/products/em/simplorer, [online], visited on April 8th 2010.

[20] Duncan Grisby, Apasphere Ltd, "omniORB – a robust high performance CORBA ORB for C++ and Python," http://omniorb.sourceforge.net, [online], visited on July 14th, 2008.

[21] S. Nabeta, I. Chabu, L. Lebensztajn, D. Correa, W. da Silva, and K. Hameyer, "Mitigation of the torque ripple of a switched reluctance motor through a multiobjective optimization," Magnetics, IEEE Transactions on, vol. 44, no. 6, pp. 1018–1021, June 2008.

[22] The MathWorks, "Simulink - Simulation and Model-Based Design," http://www.mathworks.com/products/simulink, [online], visited on 8th, 2010.

[23] PLEXIM GmbH, "Plecs manual," http://www.plexim.com, [online], visited on April 8th, 2010.

[24] dSPACE GmbH, "dspace prototyping systems," http://www.dspace.de, [online], visited on April 10th, 2010.